Wiley
International Journal of RF and Microwave Computer-Aided Engineering
Volume 2024, Article ID 4303470, 9 pages
https://doi.org/10.1155/2024/4303470

WILEY

*Research Article*

# Frequency-Tunable SIW Band-Reject Filter with Increased Fundamental Mode Bandwidth for Spectrum Underlay Cognitive Radio

**Sreenath Reddy Thummaluru**,[1] **Rajkishor Kumar**,[2] **and Raghvendra Kumar Chaudhary**[3]

[1]*Department of Electronics and Communication Engineering, Indian Institute of Information Technology Design and Manufacturing (IIITDM), Kancheepuram, Chennai 600127, India*
[2]*School of Electronics Engineering, Vellore Institute of Technology, Vellore 632014, India*
[3]*Department of Electrical Engineering, Indian Institute of Technology Kanpur, Kanpur 208016, India*

Correspondence should be addressed to Sreenath Reddy Thummaluru; sreenath@iiitdm.ac.in

Received 20 July 2023; Revised 17 April 2024; Accepted 25 April 2024; Published 23 May 2024

Academic Editor: Bhaskar Gupta



This paper presents the design of a frequency-tunable substrate-integrated waveguide (SIW) band-reject filter, specifically for spectrum underlay cognitive radio operation. The proposed filter has a simple tuning circuit but provides a wide frequency tuning range from 2.9 to 4.4 GHz (41%). The second resonant mode has been suppressed using a simple quadrature coupling; hence, the fundamental mode bandwidth of the filter has been increased from 2.08 GHz to 3.36 GHz. Due to its wide tuning range, simple tuning circuit, and increased fundamental mode bandwidth, the proposed filter is greatly important in underlay cognitive radio construction. The second-order filter has also been developed, and its performance is analyzed with both simulation and measurement. It gives a tunable bandwidth of 41%, an insertion loss of more than 10 dB, and a fundamental mode bandwidth of 3.36 GHz. The filter performance is also analyzed after connecting it to the standard horn antenna. Finally, from the total efficiency plots, it has been concluded that the proposed filter achieves all the above advantages with a low-lossy nature.

## 1. Introduction

Using the available spectrum efficiently is one of the primary objectives in 5G communications. Cognitive radio (CR) technology plays a massive role in utilizing the spectrum efficiently [1, 2]. To give more insight, the advantages of CR technology and how it improves spectrum efficiency have been explained using Figure 1. Across the electromagnetic spectrum, different applications can be found at different frequencies. There are some instances where the users are more in number at certain frequencies/applications, and at other frequencies/applications, the number of users will be less. In general, the 4G and GSM users will be more in number than TV and military users; the same can be observed from Figure 1. In this case (Figure 1(a)), the spectrum is not utilized efficiently. After introducing the CR, the excessive 4G and GSM users can utilize TV and military frequencies for their communication; hence, the spectrum efficiency and user bandwidth will be improved. The same can be observed from Figure 1(b). From this explanation, it can be said that the spectrum efficiency and user bandwidth will be improved by using CR technology.

In the above explanation, the TV and military users can be called primary users, and the GSM/4G users who are using TV/military frequencies for their communication can be called secondary or opportunistic users. Based on how secondary users access the unallotted spectrum, the CR has been divided into three types: interweave, underlay, and

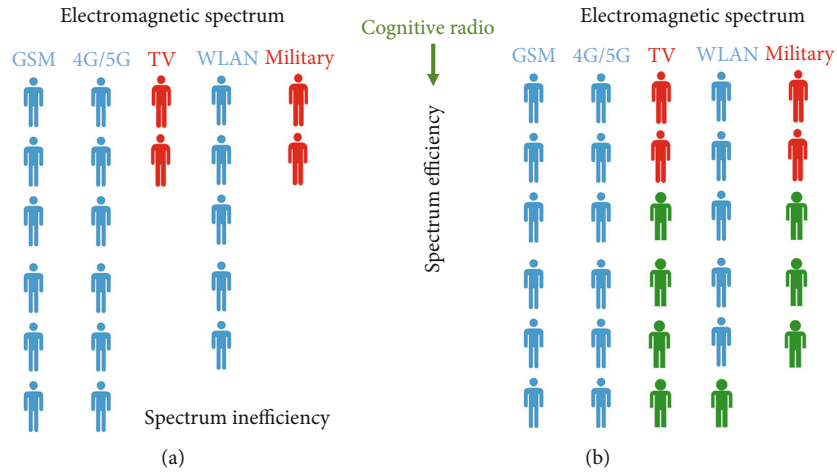


Figure 1: Electromagnetic spectrum (a) before and (b) after utilizing the cognitive radio technology.

overlay CR [3–5]. This paper concentrates only on the underlay CR. In underlay CR, the secondary users can use the entire primary users' spectrum but with a restriction that their power level should not exceed the reference level. The primary users will decide this reference power level. From the RF designer's perspective, to design the underlay CR system, a wideband antenna with frequency-tunable band notch is required [5]. To develop such kind of antenna, a frequency-tunable band-stop filter should be attached to the wideband antenna.

This paper focuses on the design of such a frequency-tunable band-stop filter. The substrate-integrated waveguide (SIW) technique has been used to develop a frequency-tunable band-stop filter. This preference is decided considering the many advantages of SIW technology over planar microstrip technology [6]. Moreover, achieving the tunable frequency property involves the lumped elements that make microstrip filters more vulnerable to losses compared to SIW filters. There are many SIW band-stop filter-based papers available in the literature [7–12]. For underlay CR, the frequency-tunable bandwidth should be as high as possible so that the secondary users can access wider frequency bandwidths. Compared to some of the SIW band-stop filters available in the literature, the frequency-tunable bandwidth of the proposed filter is wide. Moreover, the proposed filter offers two more advantages compared to the state-of-the-art; they are wide fundamental mode bandwidth and simple tuning circuit. Designing the filter with large fundamental mode bandwidth is incredibly important in underlay CR because there is a chance that the second resonant mode frequency falls in the desired sensing frequency range. Furthermore, it will create two tunable band-reject frequencies instead of one. More details about the proposed filter have been explained in the following sections.

## 2. Design Details of Band-Reject Filter

If the planar circuitry is coupled to SIW through a current probe, the band-pass filter type is output. For a voltage probe case, the band-stop filter functionality will be achieved [13]. The simple microstrip line passing through the SIW cavity, as shown in Figure 2(a), will come under voltage probe-based coupling between the microstrip line and SIW resonator. As expected, the band-stop filter property has been achieved, as shown in Figure 2(b). All the filter designs shown in this paper use Rogers RT/duroid 6002 substrate (dielectric constant = 2.94, loss tangent = 0.0012) with a thickness of 1.524 mm. The first and second resonant modes of SIW are $TE_{110}$ and $TE_{210}$, respectively. As per the selected SIW dimensions, the frequencies at which the $TE_{110}$ and $TE_{210}$ modes resonate are 4.2 GHz and 5.75 GHz, respectively, as shown in Figure 2(b). The *E*-field distributions of these two modes are shown in Figures 3(a) and 3(b). In Figure 3(a), one half-wavelength can be observed in both *x* - and *y*-directions, whereas for $TE_{210}$ mode (Figure 3(b)), two half-wavelengths in the *x*-direction and one half-wavelength in the *y*-direction can be observed. To increase the fundamental mode bandwidth, i.e., to suppress the $TE_{210}$ mode, the center coupling has been replaced by the quadrature coupling, as shown in Figure 4(a). Moreover, intentionally, the SIW dimensions are kept larger in the *x* -direction as compared to the *y*-direction ($a > b$) to put the second output port at the null position of the second mode. From Figures 3(b) and 4(a), the same can be observed; hence, the second mode gets suppressed at the output, which can be verified from its *S*-parameters, as shown in Figure 4(b).

The SIW band-reject filters that are shown in Figures 2(a) and 4(a) do not provide a strong coupling between the microstrip line and SIW cavity; hence, the insertion loss is not below 10 dB at the first mode resonant frequency for both structures, as shown in Figures 2(b) and 4(b). To improve the coupling, the step-impedance method has been adopted from [14]. The step-impedance method introduces high and low impedance sections at suitable positions to provide strong coupling [15]. Such a step-impedance-based quadrature-coupled SIW band-reject filter is shown in Figure 5(a). The via radius has been increased to reduce the via number and soldering complexity during fabrication; however, the SIW design rules are still strictly

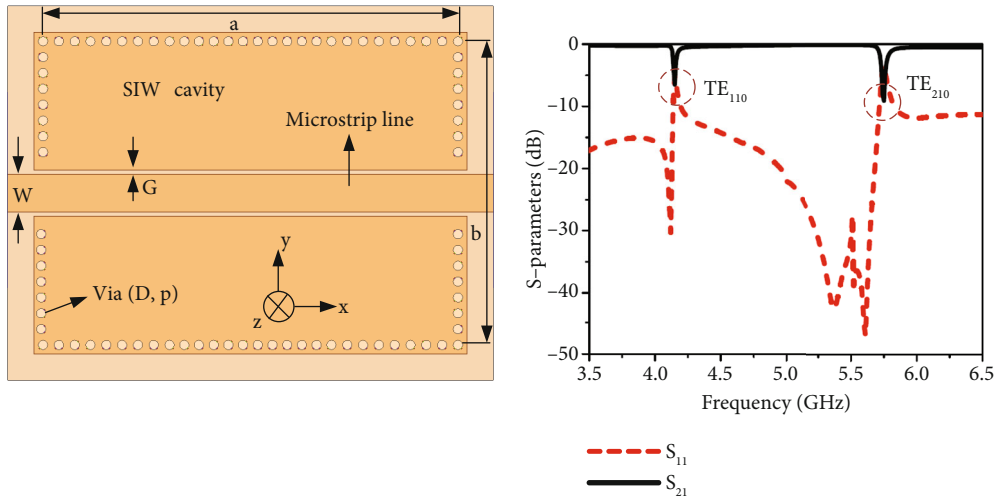


FIGURE 2: The voltage probe-based center coupling between the microstrip line and SIW resonator: (a) design and (b) band-stop filter response ($a = 44.6$, $b = 32.6$, $D = 1$, $p = 1.7$, $G = 0.5$, and $W = 4$; all dimensions are in mm. $D$ = via diameter; $p$ = distance between two via centers).

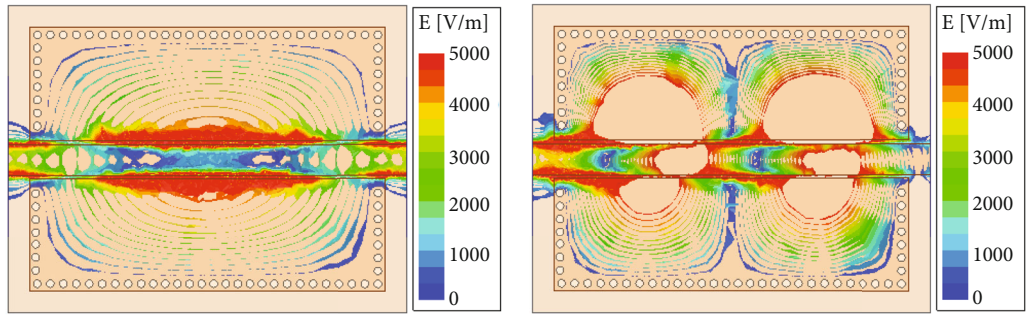


FIGURE 3: The $E$-field distributions: (a) $TE_{110}$ and (b) $TE_{210}$ modes.

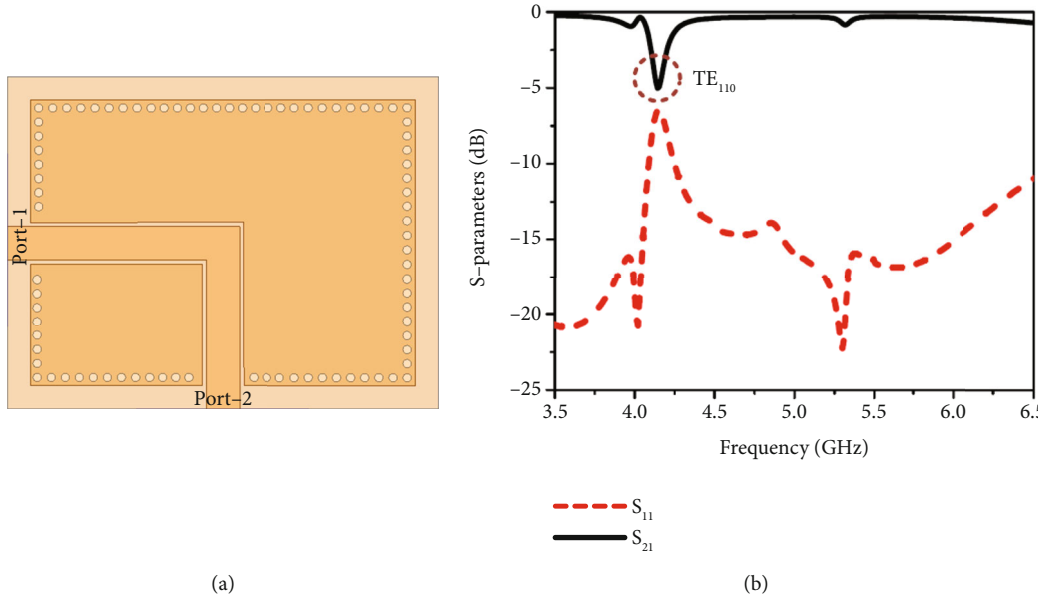


FIGURE 4: The voltage probe-based quadrature coupling: (a) design and (b) simulated $S$-parameters.

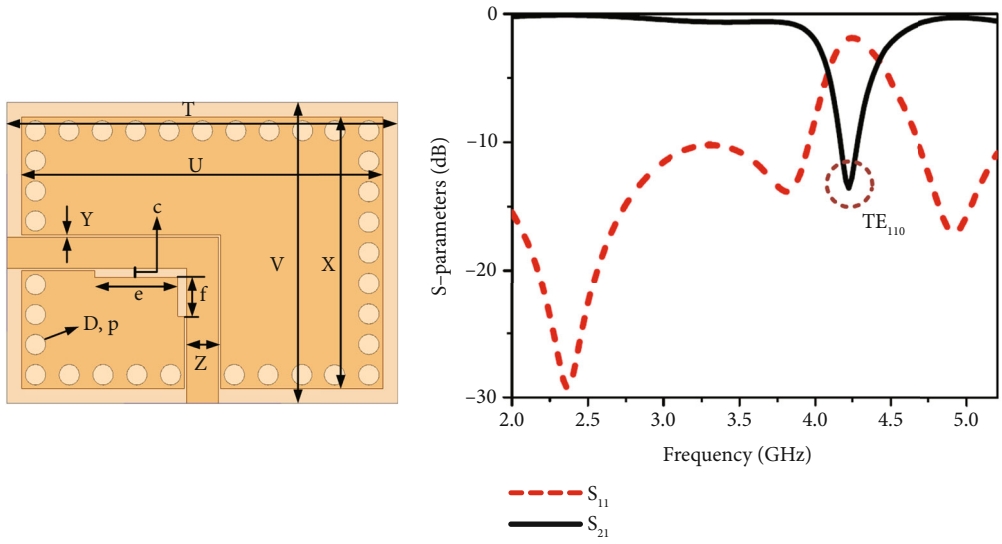


FIGURE 5: The proposed band-reject filter: (a) design and (b) simulated $S$-parameters ($c = 1.2$, $e = 11.1$, $f = 5.2$, $D = 2.7$, $p = 4$, $T = 52.2$, $U = 48.3$, $V = 40.2$, $X = 36.3$, $Y = 0.3$, and $Z = 4.2$; all dimensions are in mm).

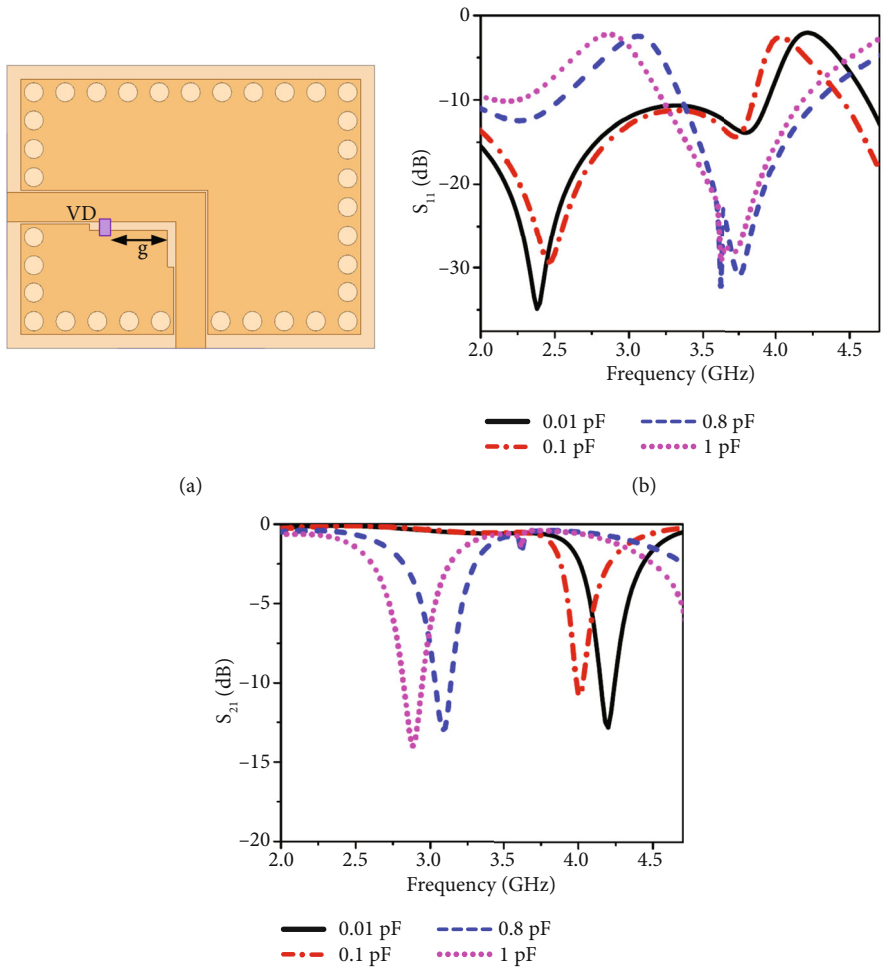


FIGURE 6: The proposed band-reject filter with a varactor diode (VD): (a) design, (b) simulated input reflection coefficient, and (c) simulated $S_{21}$ at different reverse bias VD capacitances.

Table 1: Comparison of a proposed filter with the state-of-the-art.

| | Details | Number of diodes | Tuning range |
|---|---|---|---|
| [7] | Dual-band-stop filter with one tunable stopband | 2 | 3.5-4.1 GHz (15%) |
| [8] | Frequency and bandwidth tunable band-stop filter | 2 | 2.8-3.4 GHz (19.3%) |
| [9] | *X*-band tunable band-stop filter | 2 | 10.02-10.34 GHz (3.1%) |
| [10] | Half-mode band-stop filter | 1 | 2-2.5 GHz (22.2%) |
| [11] | Coaxial band-stop filter | 2 | 0.77-1.25 GHz (47%) |
| [12] | Octave tunable combline band-stop filter | 12 | 0.56-1.18 GHz (71%) |
| This work | Band-stop filter with high fundamental mode bandwidth | 1 | 2.9-4.4 GHz (41%) |

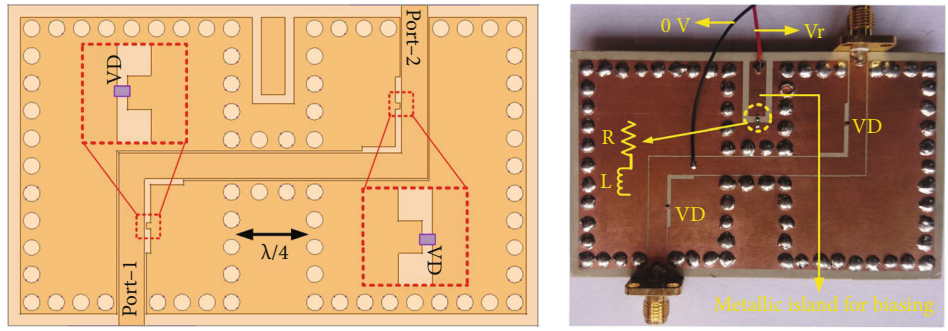


(a) (b)

Figure 7: The second-order band-reject filter: (a) simulated design and (b) fabricated structure.

followed. From its *S*-parameters, which are shown in Figure 5(b), the increase in the insertion loss (>10 dB) at $TE_{110}$ resonant frequency of 4.2 GHz can be observed.

The next step in the design process is to make the band-reject frequency tunable over a wide range. To accomplish that, a varactor diode (VD) has been introduced in the band-reject filter structure, as shown in Figure 6(a). Since the step impedance decides the coupling between the microstrip line and SIW cavity, the VD should be introduced within the step-impedance section to make the band-rejection frequency tunable. It must be noted that many optimizations are done using HFSS software to determine the exact position of VD within the step-impedance section. The simulated $S_{11}$ and $S_{21}$ are shown at different reverse bias VD capacitances in Figures 6(b) and 6(c), respectively. From these figures, the tunable frequency property of the proposed filter is evident. The tunable frequency range is from 2.9 to 4.4 GHz. In terms of percentage, it is approximately 41%. It was discussed in the introduction section that this paper is aimed at designing the band-reject filter for underlay CR application. It was also discussed that the tunable frequency range of the band-reject filter should be as high as possible for underlay CR operation. The proposed filter offers a wider tuning range compared to some of the already available SIW band-reject filters in the literature. The same can be observed from the comparison table (Table 1). The band-stop filters present in [11, 12] offer more tuning range compared to the proposed structure; however, the fundamental mode bandwidth of the proposed band-reject filter is high as compared to the filters in [11, 12]. Moreover, the number of diodes used in [12] to achieve tunable property is very large.

Table 2: The series RLC values of MAVR-011020-1411 at different biasing voltages.

| Biasing voltage | Resistor ($R$) | Inductor ($L$) | Capacitor ($C$) |
|---|---|---|---|
| 0 V | 1.7 Ω | 0.7 nH | 0.25 pF |
| 1 V | 1.7 Ω | 0.7 nH | 0.18 pF |
| 3 V | 1.7 Ω | 0.7 nH | 0.09 pF |
| 6 V | 1.7 Ω | 0.7 nH | 0.06 pF |
| 10 V | 1.7 Ω | 0.7 nH | 0.04 pF |

## 3. Second-Order Band-Reject Filter and Its Application in Spectrum Underlay CR

For underlay CR, a wideband antenna with the frequency-tunable band notch is required. The band notch frequency is where the secondary users stop their communication since it creates interference with primary users' communication [16, 17]. The selectivity of the band notch should be good for better underlay CR operation. Thus, the second-order band-reject filter has been designed by cascading the two single-order proposed band-reject filters, as shown in Figure 7(a). The quarter-wave line, which acts like a nonresonating node, has been used for cascading the two single-order filters. The fabricated second-order band-reject filter along with VD is shown in Figure 7(b). The VD used in our design is MAVR-011020-1411 from MACOM Technology Solutions. The VD capacitances are taken from its datasheet [18]. The series RLC circuit is used in the simulations

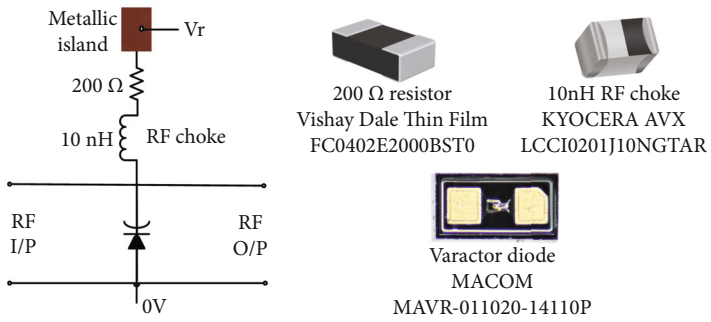


FIGURE 8: The biasing circuit to control the varactor diode along with the enlarged views of resistor, inductor, and varactor diode.

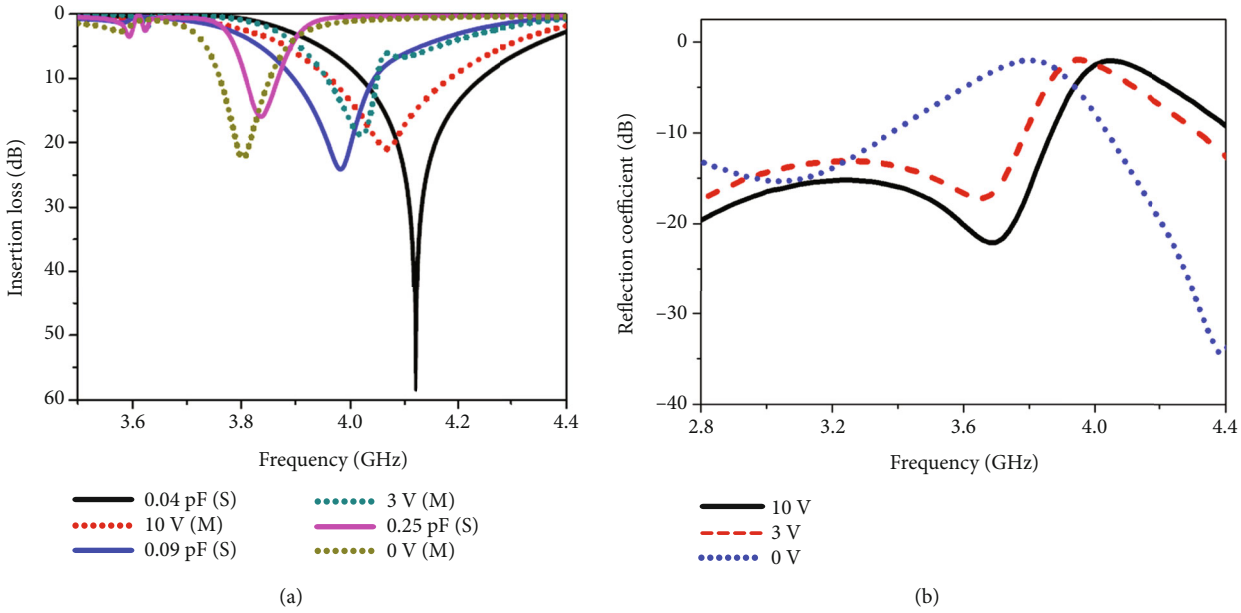


FIGURE 9: (a) Simulated and measured insertion loss and (b) measured reflection coefficient of second-order filter at different biasing voltages ("*S*" means simulated and "*M*" means measured).

to replicate VD. The RLC values of MAVR-011020-1411 at different biasing voltages are shown in Table 2. The capacitance of the varactor diode depends on its reverse bias voltage, as shown in Equation (1), where $C(\mathrm{Vr})$ is the capacitance of varactor diode, Cp is the parasitic capacitance, $C_{J0}$ is the PN junction capacitance at zero bias, $M$ is the constant, Vj is the junction potential, and Vr is the reverse bias voltage.

$$C(\mathrm{Vr}) = \frac{C_{J0}}{(1 + (\mathrm{Vr}/\mathrm{Vj}))^{M}} + \mathrm{Cp}. \quad (1)$$

To get different capacitances from the varactor diode, it has to be connected in the reverse bias with one end to zero voltage and another to DC supply. Along with the DC supply, a resistor and inductor have to be incorporated to complete the biasing circuit for the varactor diode. The inductor acts like an RF choke by preventing the flow of RF current into the DC supply and thus protecting it. The resistor limits the current flow through the varactor diode. The inductor and resistor can be connected either externally through a simple copper wire or internally by soldering them on the PCB itself. To connect them internally, we have created a metallic island on the PCB, as shown in Figure 7(b). A DC supply (Vr) is given to the metallic island by soldering a copper wire on it. The resistor and inductor are connected between the DC supply and cathode terminal of varactor diode. The complete DC biasing circuit, along with the enlarged views of the resistor, inductor, and varactor diode, is given in Figure 8.

The simulated and measured insertion loss has been compared in Figure 9(a). This VD reverse bias capacitance varies only from 0.25 pF to 0.04 pF; hence, it became impossible for us to show the entire tuning range of the proposed filter, i.e., 2.9-4.4 GHz by measurement. If MA46H120 from MACOM is used as VD, then it should have been possible to show most of the tuning range of 2.9-4.4 GHz. Unfortunately, MA46H120 is not available with us. There are some notable differences between the simulated and measured

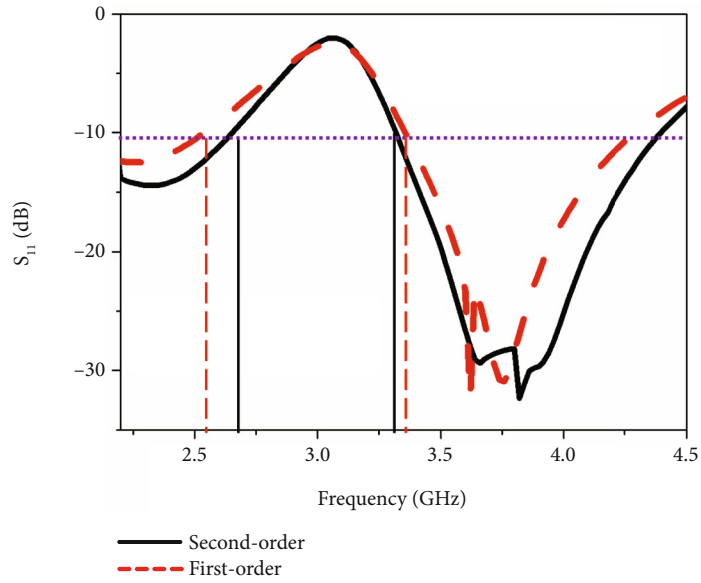


Figure 10: Simulated reflection coefficient of the first- and the second-order filter at VD capacitance of 0.8 pF.

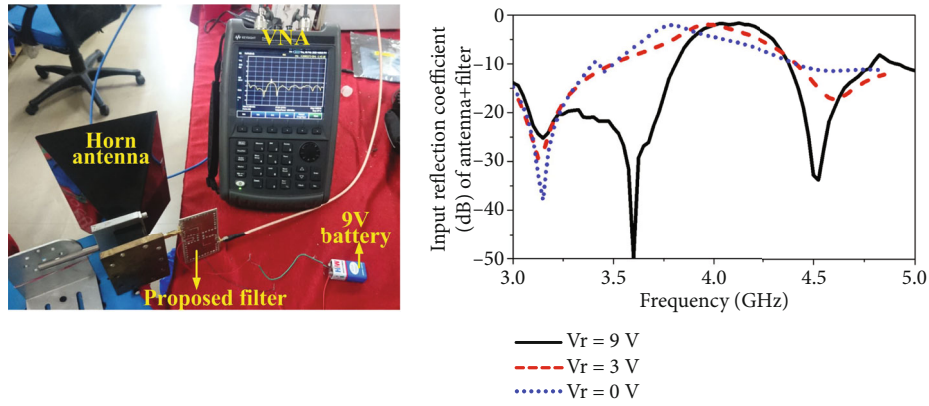


Figure 11: The proposed filter is connected with the horn antenna: (a) measurement setup and (b) measured input reflection coefficients at different biasing voltages.

results due to the fabrication and soldering imperfections. The measured reflection coefficients at various biasing voltages are given in Figure 9(b). Figures 9(a) and 9(b) confirm the tunable property of the second-order filter. The second-order filter response is also compared with the first-order filter response in Figure 10 to observe the improvement in selectivity and low return loss.

The proposed filter can be employed in the underlay CR operation. Please note that in this paper, an underlay CR system, which includes the specialized wideband antenna and other digital signal processing units, is not designed separately. To just explain the usefulness of the proposed filter in underlay CR, the designed filter is connected to the horn antenna and estimated the input reflection coefficient by measurement. The same can be observed in Figure 11(a). The impedance bandwidth of the horn antenna is 2.6-4.6 GHz. It is known that a wideband antenna with a tunable band notch is required for underlay CR operation. By connecting the proposed filter with any wideband antenna, the required antenna type can be achieved for underlay CR operation. After connecting the proposed filter with the horn antenna, the reflection coefficient, as shown in Figure 11(b), has been achieved. It can be observed that the band notches occurred at different frequencies by changing the biasing voltages. Readers may wonder how this filter is advantageous compared to the already available SIW band-reject filters, particularly for underlay CR operation. The explanation is that the proposed filter has a suppressed second mode, i.e., $TE_{210}$ mode. For example, if any other filter whose second mode resonant frequency falls in the desired wideband antenna bandwidth, then instead of a single tunable band notch, there exists a double tunable band notch, which does not support underlay CR operation. In addition, the proposed filter has a simple biasing circuit with a smaller number of lumped elements, which accounts for low losses compared to the state-of-the-art filters. To verify this, the

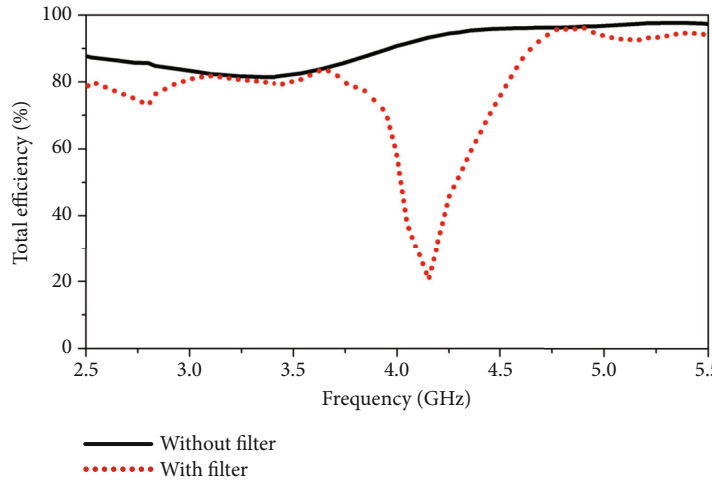


Figure 12: The simulated total efficiency of the antenna before and after connecting to the filter.

simulated total efficiency of the antenna and antenna+filter has been given in Figure 12. Please note that the total efficiency of the antenna with filter is provided at Vr = 9 V. Except at the band notch frequency of 4.1 GHz, the difference between the efficiencies of both cases is minimal, which suggests the low-lossy nature of the proposed filter.

## 4. Conclusion

The design of the substrate-integrated waveguide-tunable filter for underlay cognitive radio system has been presented in this paper. The design procedure started with the single-order tunable band-reject filter design, and it was followed by a discussion on the second-order filter design, its fabrication details, and measurement results. Finally, the proposed filter is connected to the horn antenna, and the overall performance has been estimated. Considering the advantages like wide tunable range from 2.9 to 4.4 GHz, simple biasing circuit, a smaller number of lumped elements, insertion loss of more than 10 dB, and fundamental mode bandwidth of 3.36 GHz, it can be said that the proposed filter is a suitable candidate for underlay cognitive radio applications.

## Data Availability

The data that support the findings of this study are available from the corresponding author upon reasonable request.

## Conflicts of Interest

The authors declare that they have no conflicts of interest.

## Acknowledgments

The authors acknowledge the Science and Engineering Research Board (SERB), DST, Government of India, for the partial financial support under grant no. EEQ/2021/000077. The authors also want to thank the Indian Institute of Information Technology, Design and Manufacturing, Kancheepuram, for the financial support through SMIRE project number IIITDM/SMIRE/2023/005.

## References

[1] M. Al-Husseini, K. Y. Kabalan, A. EI-Hajj, and C. G. Christodoulou, "Reconfigurable microstrip antennas for cognitive radio," in *Advancement in Microstrip Antennas with Recent Applications*, pp. 337–362, IntechOpen, Ahmed Kishk, Croatia, 2013.

[2] T. A. Khalaf, M. Y. Abdelsadek, and M. Farrag, "Compressed measurements based spectrum sensing for wideband cognitive radio systems," *International Journal of Antennas and Propagation*, vol. 2015, Article ID 654958, 7 pages, 2015.

[3] Y. Tawk, J. Costantine, and C. G. Christodoulou, "Reconfigurable filtennas and MIMO in cognitive radio applications," *IEEE Transactions on Antennas and Propagation*, vol. 62, no. 3, pp. 1074–1083, 2014.

[4] S. Emam and M. E. Celebi, "Non-orthogonal multiple access protocol for overlay cognitive radio networks using spatial modulation and antenna selection," *AEU–International Journal of Electronics and Communication*, vol. 86, pp. 171–176, 2018.

[5] S. R. Thummaluru, M. Ameen, and R. K. Chaudhary, "Four-port MIMO cognitive radio system for mid-band 5G applications," *IEEE Transactions on Antennas and Propagation*, vol. 67, no. 8, pp. 5634–5645, 2019.

[6] X.-P. Chen and K. Wu, "Substrate integrated waveguide filter: basic design rules and fundamental structure features," *IEEE Microwave Magazine*, vol. 15, no. 5, pp. 108–116, 2014.

[7] M. Esmaeili and J. Bornemann, "Novel tunable bandstop resonators in SIW technology and their application to a dual-bandstop filter with one tunable stopband," *IEEE Microwave and Wireless Components Letters*, vol. 27, no. 1, pp. 40–42, 2017.

[8] S.-W. Jeong and J. Lee, "Frequency- and bandwidth-tunable bandstop filter containing variable coupling between transmission line and resonator," *IEEE Transactions on Microwave Theory and Techniques*, vol. 66, no. 2, pp. 943–953, 2018.

[9] M. Cariou, S. Cadiou, B. Potelon, C. Quendo, R. Segalen, and F. Mahe, "New tunable substrate integrated waveguide

bandstop resonator," in *2016 IEEE MTT-S Latin America Microwave Conference (LAMC)*, Puerto Vallarga, Mexico, 2016.

[10] J. Hinojosa, A. Saura-Rodenas, A. Alvarez-Melcon, and F. L. Martinez-Viviente, "Reconfigurable coplanar waveguide (CPW) and half-mode substrate integrated waveguide (HMSIW) band-stop filters using a varactor-loaded metamaterial-inspired open resonator," *Materials*, vol. 11, no. 1, pp. 17–39, 2018.

[11] A. Anand and X. Liu, "Capacitively tuned electrical coupling for reconfigurable coaxial cavity bandstop filters," in *2015 IEEE MTT-S International Microwave Symposium*, Phoenix, AZ, USA, 2015.

[12] A. Anand, Y. Liu, and X. Liu, "Substrate-integrated octave-tunable combline bandstop filter with surface mount varactors," in *2014 IEEE international wireless symposium (IWS 2014)*, Xian, China, 2014.

[13] Y. Cassivi, L. Perregrini, K. Wu, and G. Conciauro, "Low-cost and high-Q millimeter-wave resonator using substrate integrated waveguide technique," in *32nd European Microwave Conference*, Milan, Italy, 2002.

[14] B. H. Ahmad and I. C. Hunter, "Design and fabrication of a substrate integrated waveguide bandstop filter," in *38th European Microwave Conference*, Amsterdam, Netherlands, 2008.

[15] I. C. Hunter, *Theory and Design of Microwave Filter*, The Institution of Electrical Engineers, 2001.

[16] T. Alam, S. R. Thummaluru, and R. K. Chaudhary, "Improved multi-functional MIMO cognitive radio system for integrated interweave-underlay operations," *IEEE Transactions on Microwave Theory and Techniques*, vol. 70, no. 1, pp. 631–640, 2022.

[17] V. Aswathi and A. V. Babu, "Performance analysis of NOMA-based underlay cognitive radio networks with partial relay selection," *IEEE Transactions on Vehicular Technology*, vol. 70, no. 5, pp. 4615–4630, 2021.

[18] "MAVR-011020-14110P datasheet, MACOM Technology Solutions, Inc., USA," https://www.mouser.in/datasheet/2/249/MAVR_011020_1141-911318.pdf.